DOI 10.1007/s11141-023-10212-8
Radiophysics and Quantum Electronics, Vol. 65, No. 4, September, 2022
(Russian Original Vol. 65, No. 4, April, 2022)

3D-PRINTED PHASE WAVE PLATES FOR CREATION OF TERAHERTZ BEAMS WITH LINEAR POWER DISTRIBUTION

K. R. Dzhikirba,[1,2] * **P. A. Gusikhin,**[1,3]
V. M. Murav'ev,[1,3] **I. V. Kukushkin,**[1,3]
J. Gospodarič,[4] **and A. Pimenov**[4]

UDC 53.06

We calculate the profile of a phase plate for an operating frequency of 100 *GHz, which allows one to obtain a beam with the most uniform power distribution in the region* 384×6 *mm at a distance of* 50 *cm, using the Gerchberg–Saxton iterative algorithm. A series of phase plates made of polyamide was 3D-printed. The parameters of the phase plate measured experimentally agree well with the theoretical calculations. The depth resolution of the image and the dependence of the beam profile on the frequency of the incident radiation are also studied. The obtained results are of practical use in the field of nondestructive control for the creation of linear terahertz scanners.*

1. INTRODUCTION

Growing interest in systems operating in the terahertz frequency range (0.1–3.0 THz) is related to various applications in the safety and nondestructive control field [1, 2]. Imaging in the above-specified range is a promising method of detecting defects within objects that are opaque in the visible light range. Remote terahertz inspection is becoming a popular approach to ensuring safety of airports and railway stations [3, 4]. The wavelength of terahertz waves is shorter as compared to radio waves, which allows one to obtain images with high spatial resolution. Most of the materials (plastic, wood, and ceramics) are still transparent in the terahertz frequency range [5]. Another major advantage of terahertz waves, as compared with X-rays, is that the terahertz radiation is non-ionizing and, therefore, safe for humans.

At present, there are several methods of terahertz imaging [6, 7, 8]. The first developed method was terahertz time-resolved spectroscopy [9, 10]. Raster scanning is used to obtain images in such systems. Despite the proven efficiency, time-resolved scanning systems are still costly and difficult to operate. Another method is based on irradiation of the considered specimen with terahertz waves at a fixed frequency with further analysis of the spatial distribution of the transmitted-radiation power. Earlier, it was done by the method of slow raster scanning. Recently, there have been significant advances in the field of development of detector matrices based on microbolometers, silicon metal–oxide–semiconductor (MOS) circuits, pyroelectric devices, and high-electron-mobility transistors [11, 12, 13, 14]. These matrices make it possible to obtain terahertz images at a high rate but, up to recently, it has been impossible to achieve good spatial resolution in them due to a small number of detectors in the matrix.

Recently, a linear terahertz scanner has been developed, which operates at a frequency of 100 GHz and has a sensitive region with a total size equal to 400×3 mm [15]. It is capable of measuring simultaneously

* ki805rill@mail.ru

[1] Institute of Solid State Physics of the Russian Academy of Sciences, Chernogolovka; [2] Moscow Physico-Technical Institute (National Research University), Dolgoprudny, Russia; [3] TeraSense Group Inc., San Jose, USA; [4] Vienna University of Technology, Vienna, Austria. Translated from Izvestiya Vysshikh Uchebnykh Zavedenii, Radiofizika, Vol. 65, No. 4, pp. 314–322, April 2022. Russian DOI: 10.52452/00213462_2022_65_04_314 Original article submitted November 27, 2021; accepted April 28, 2022.

a signal from 256 detectors situated in one line in 0.2 ms. If the considered object is moved across the linear scanner by means of a conveyor, it is possible to obtain the spatial pattern of terahertz radiation transmission through bulk objects in real time. In this case, a spatial resolution of 3 mm is achieved. One of the most important technical issues of the linear terahertz scanner is the necessity of organizing uniform illumination of the working window of the camera. Currently, a sophisticated system of lenses or parabolic mirrors is used for this purpose. Similarly to classical optics, there are various elements allowing one to control the shape and intensity of the beam.

Fig. 1. Schematic for achievement of the required profile of intensity distribution. The source is an avalanche transit-time diode with a radiation frequency of 97 GHz.

An example of such elements is subwave metasurfaces, which allow one to minimize the size of the optical system efficiently [16, 17]. Another variant is based on the use of diffraction optical elements [18, 19]. The holographic plates, which are produced in this way, make it possible to manipulate the beam effectively. A specific advantage of this approach is the possibility to calculate elements in the terahertz frequency range, since the Maxwell equations, which underlie the calculations, do not contain the wavelength as a parameter. A special case is the plates that use only a phase modulation to control the beam [20, 21, 22]. Such elements are called phase holograms. Well-known examples of phase holograms are dielectric Fresnel lenses and dielectric diffraction gratings.

Our objective was to use the method of 3D printing to create a phase plate which focuses terahertz radiation to an elongated area with a size of 400×3 mm at a given distance from the plate surface. A prototype of the device shown in Fig. 1 has successfully been manufactured and studied. It has been shown that an advantage of the proposed approach is the ease of manufacturing phase plates, a small size of the operating configuration, and high efficiency of scanner illumination.

2. TECHNICAL DESCRIPTION

The objective of this work is to convert an electromagnetic beam with the Gaussian power distribution at a frequency of 97 GHz to a uniformly illuminated rectangular 384×6 in size at a distance of 50 cm from the radiation source. Such a power distribution profile is required for uniform illumination of linear arrays of terahertz detectors. An avalanche transit-time diode (ATTD), an oscillator manufactured by the TeraSense company and producing a power of 80 mW, was used as a source. In order to solve this problem, we have developed, manufactured (using 3D printing), and studied a phase plate.

The Gerchberg–Saxton iterative algorithm [23] was used to determine the required shape of the wave plate. In order to convert the initial beam to the required one, the phase profile in the plane of the plate was determined from the intensity distribution in the far field. The Gerchberg–Saxton algorithm employs the Fourier transform to relate the electromagnetic-field profiles in the diffraction plane and the image plane. We have modified this algorithm by establishing new relationships required in our case. To do this, we used the Huygens principle, which states that each point with the coordinates (x, y) in the diffraction plane is a source of a spherical wave contributing to the electric field in the image plane at the point (x', y'):

$$E^{\mathrm{d}}_{(x,y)}(x', y') = \frac{A_{(x,y)}}{r_{(x,y).(x',y')}} \exp[-ikr_{(x,y).(x',y')} + i\phi_{(x,y)}]. \tag{1}$$

Here, $r_{(x,y).(x',y')}$ is the distance between the point (x, y) in the diffraction plane and the point (x', y') in the image plane, k is the wave number, and $A_{(x,y)}$ and $\phi_{(x,y)}$ are the amplitude and phase of the wave,

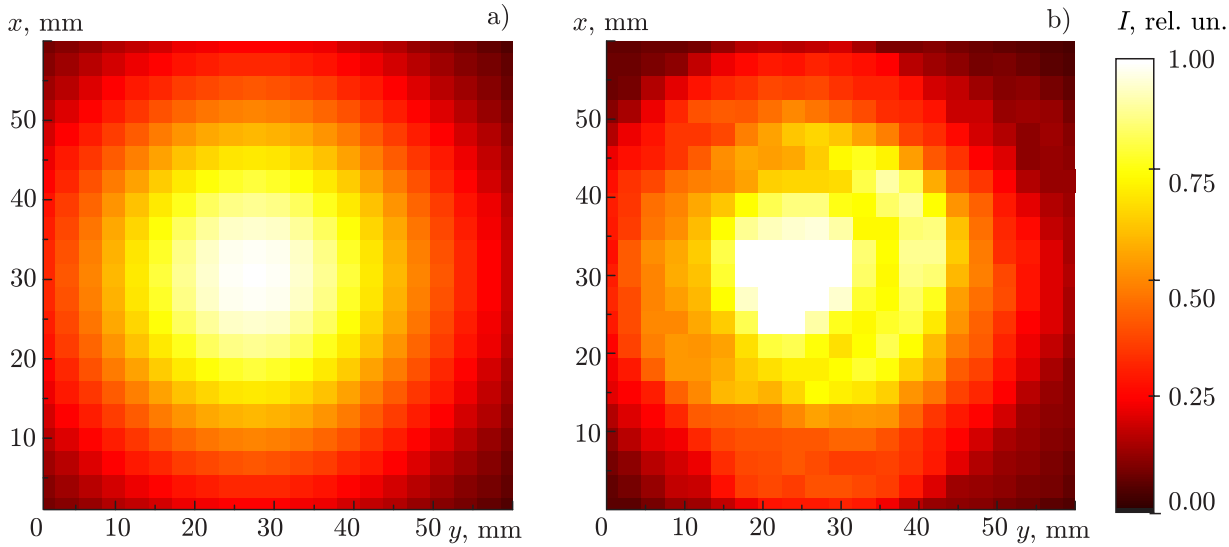

Fig. 2. Theoretical distribution of the field intensity I (*a*), which was used for calculations, and the experimentally measured distribution of the intensity at the output from the source with a conical horn at a distance of 75 mm (*b*). It is evident that the Gaussian beam in panel *b* is imperfect and has a slight shift of the intensity maximum to the left.

respectively. The resulting distribution of the field in the image plane is yielded by interference of all waves:

$$E^{\mathrm{i}}_{(x',y')} \propto \sum_{(x,y)} E^{\mathrm{d}}_{(x,y)}(x',y')(1+\cos\Omega). \tag{2}$$

Here, Ω is the angle between the optical axis of the system and the straight line connecting the points (x,y) and (x',y'). Sequential transmission of the wave in the forward and backward directions are used in the Gerchberg–Saxton algorithm. Therefore, the diffraction and image planes interchange their places for the second step in the above formulas.

The actual phase plate was illuminated by an ATTD source with a conical horn at the output, which produced a near-Gaussian distribution of the output electric field:

$$E(x,y) \propto \frac{1}{2\pi w^2} \exp\left[-\frac{x^2+y^2}{4w^2} + \frac{2i\pi}{\lambda}\left(\sqrt{l^2+x^2+y^2}-l\right)\right], \tag{3}$$

where l is the distance between the output of the horn antenna and the plane of the phase plate, w is the effective width of the Gaussian beam in the plane of the phase plate, and λ is the radiation wavelength. The optimal distance between the horn output and the phase plate, at which the distribution of the intensity in the image plane will be as close as possible to the uniform one, is $l = 75$ mm. The distribution of the source radiation power, which was measured at this distance, is presented in Fig. 2*b*. Based on it, one can find the beam width $w = 15.7$ mm, which was used further to calculate the phase plate (see Fig. 2*a*). Then we performed simulation to obtain a maximally narrow and, at the same time, intensity-uniform beam with a width of 40 cm in the image plane at a distance of 50 cm from the phase plate. The obtained profile of the phase distribution $\phi(x,y)$ is shown in Fig. 3. The thickness of the phase plate at the point with the coordinates (x,y) was determined as

$$z(x,y) = \frac{\phi(x,y)\lambda}{2\pi(n-1)}, \tag{4}$$

where n is the refractive index of the plane material. The 3D printing technology was used to manufacture the plate. Prior to that, we tested several materials for 3D printing. Allowing for the required printing quality and the terahertz loss, we have chosen polyamide. Its refractive index is equal to $n = 1.6$ at a

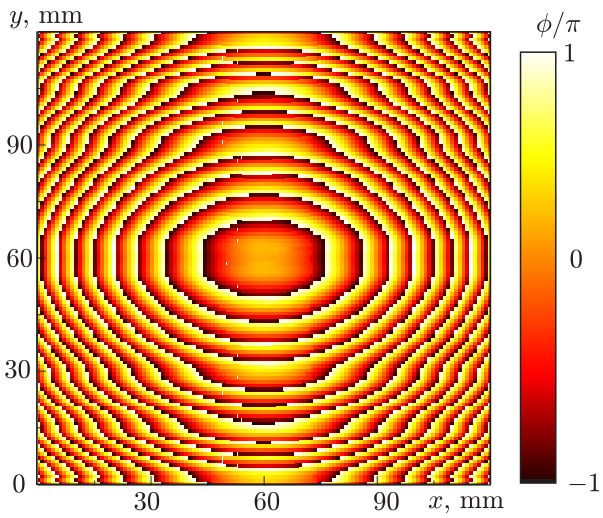

Fig. 3. Profile of the phase distribution $\phi(x, y)$ at the output from the wave plate.

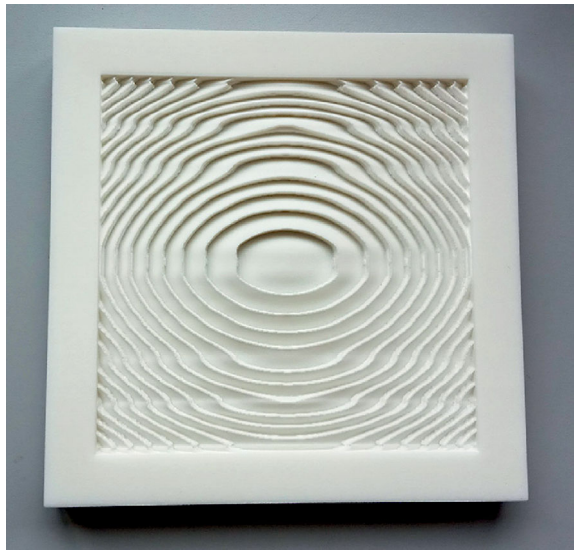

Fig. 4. Photo of the 3D-printed polyamide plate.

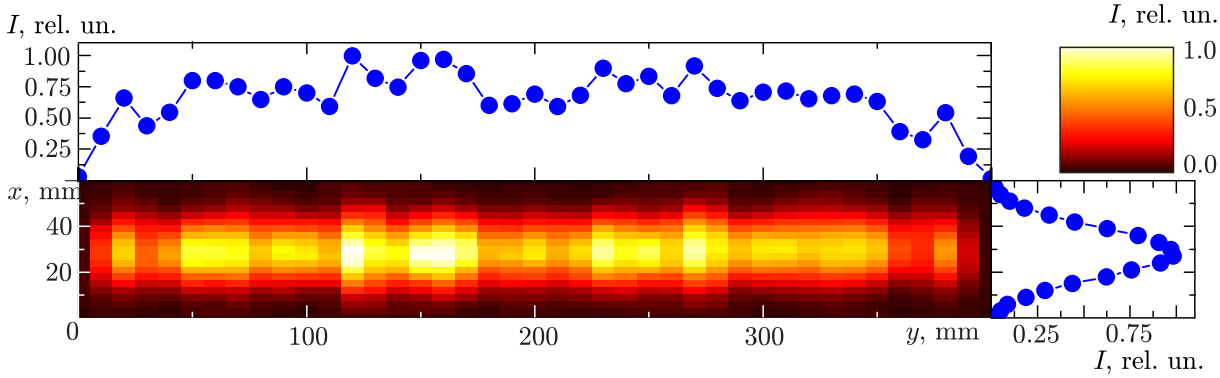

Fig. 5. Distribution of the intensity I in the image plane after the radiation has passed through the phase plate. The distance between the plate and the detector is 500 mm. The left top and right bottom panels show the profiles of the intensity distribution at $x = 30$ mm and $y = 160$ mm, respectively.

frequency of 97 GHz, which is of interest to us, and the loss tangent is 0.008. The printing was performed by the method of selective laser sintering. The resolution along each direction was 0.1 mm. A photo of the 3D-printed plate is shown in Fig. 4.

3. MEASUREMENT RESULTS

A pyroelectric detector installed on a two-axis movable table was used to measure the field distribution in the image plane. The size of the sensitive crystal was 4×4 mm, which determined the minimum sensible scanning pitch. The signal from the detector was fed to a synchronous amplifier with an externally modulation at a frequency of 23 GHz. First, similarly to the calculations, the distance between the source and the wave plate was optimized, in order to achieve the most uniform illumination of the region of interest. The distance obtained in the experiment by adjusting coincided with a theoretically found value of 75 mm. Then, pointwise scanning of the beam profile was performed at a distance of 50 cm from the wave plate (i.e., in the image plane). The measurement results are shown in Fig. 5. One can see a certain nonuniformity in the distribution of the intensity between the left-hand and right-hand sides, which can be explained by the asymmetry of the beam produced by the ATTD source (see Fig. 2*b*). Despite the fact that such defects were not allowed for during numerical simulation, it is evident that the results agree well with the theoretical calculations.

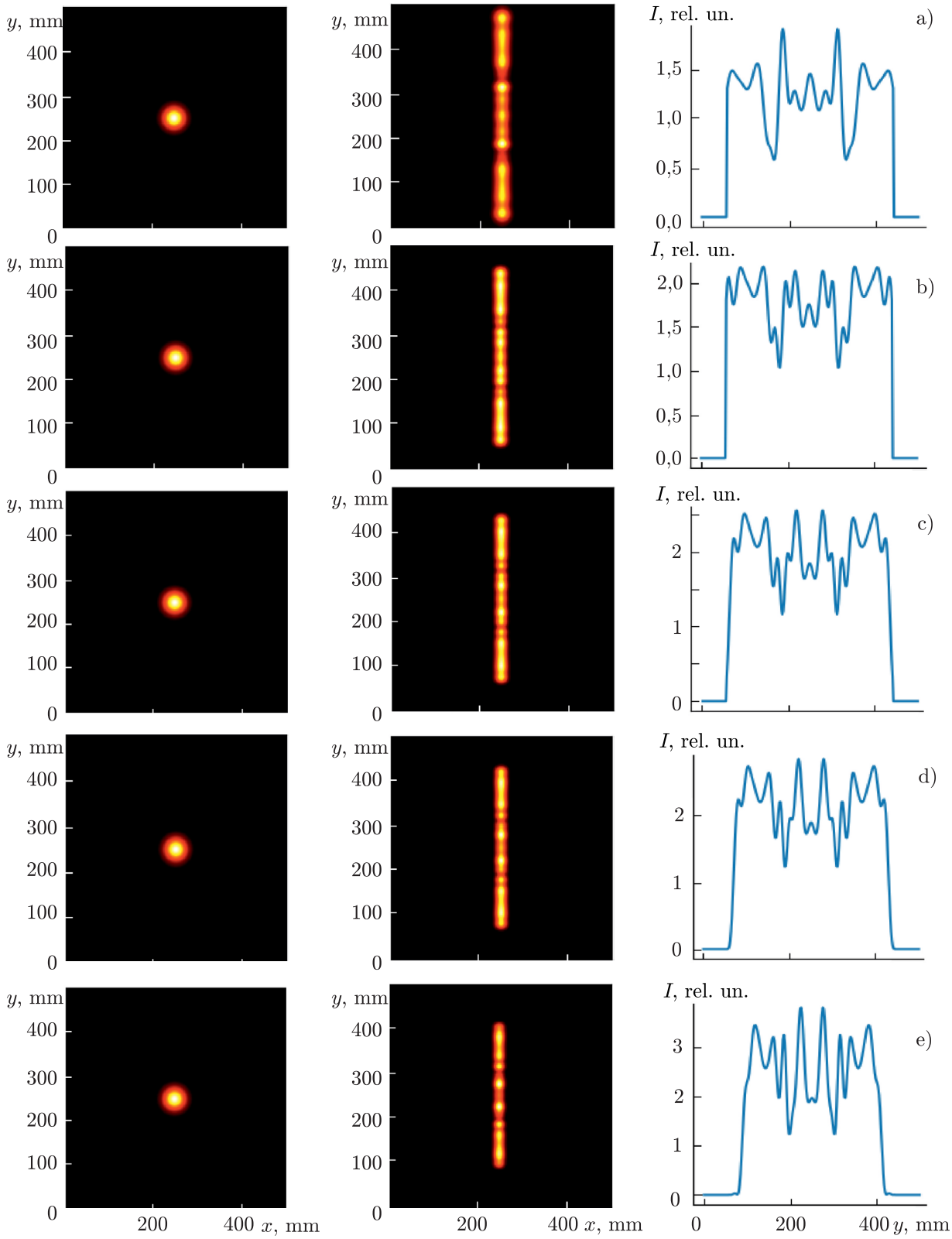

Fig. 6. Intensity distributions of the radiation incident on the plate (central column) at the frequencies 80 GHz (*a*), 92 GHz (*b*), 97 GHz (*c*), 100 GHz (*d*), and 110 GHz (*e*). The profile of the incident beam (the left column) was identical in all the cases. The right column shows the distribution of the intensity at the symmetry axis of the obtained pattern.

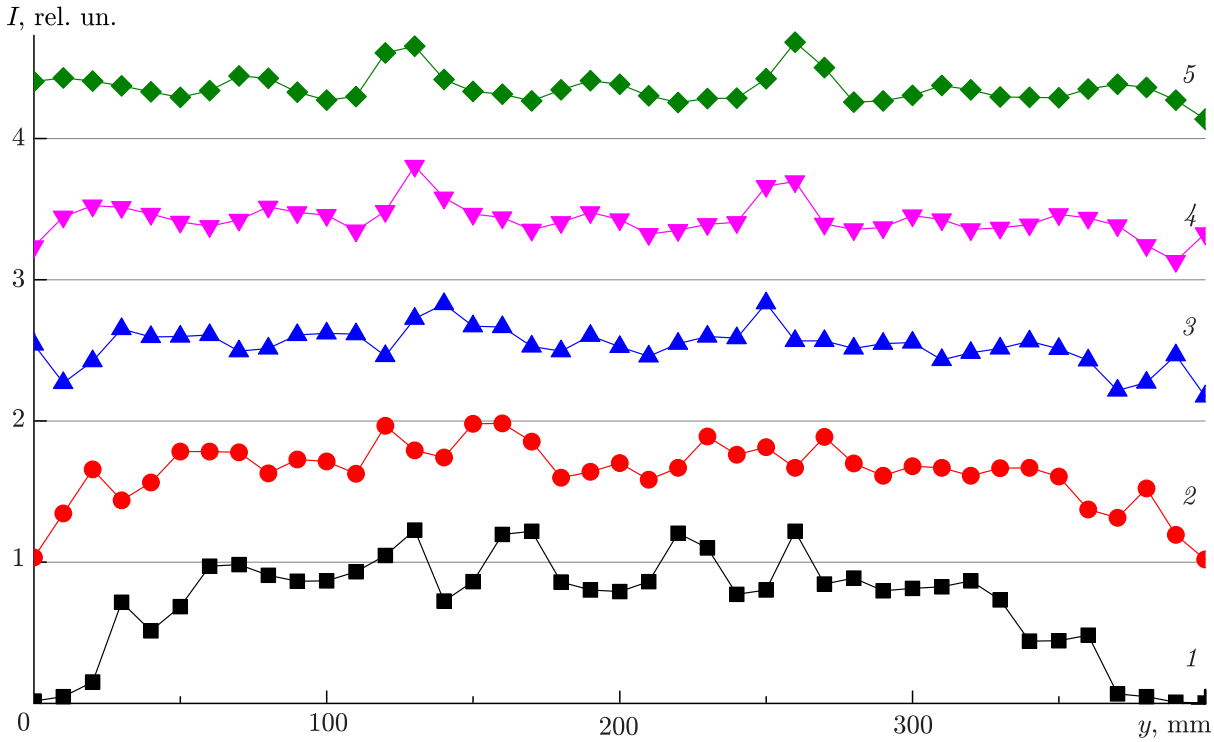

Fig. 7. Depth resolution for different distances between the wave plate and the image plane: 450 mm (*1*), 500 mm (*2*), 550 mm (*3*), 600 mm (*4*), and 650 mm (*5*). For clarity, each subsequent curve is shifted upwards to $I = 1$ rel. un. with respect to the previous one.

We also performed measurements for ATTD sources at different frequencies in the range 96–97 GHz. In this frequency range, the phase plate demonstrated stability of the intensity distribution. It is evident from the theoretical calculations (see Fig. 6) that the wave front turns out to be sufficiently stable in a wider frequency range, specifically, 92–100 GHz. Additionally, we have studied how the shape of the beam (i.e., the depth resolution of the image) changes as the distance between the wave plate and the image plane varies (see Fig. 7). One sees that in the distance range 45–65 cm, the profile of the beam retained its shape, and the intensity distribution varied only slightly.

It should be noted that despite the high efficiency of illumination of the working region, which was demonstrated, the phase plate technology has some drawbacks. We have found that the total transmission of the radiation through the plate was only 61% (in terms of the radiation power). Such losses can be due to several reasons. First, absorption in the material of the wave plate is amplified by the surface texture. Second, the reflection, which is caused by the shape of the plate and the total internal reflection, turns out to be exceedingly strong as compared with the calculated five-percent absorption level. This issue determines the way for improving and developing the proposed technology further.

4. CONCLUSIONS

In this paper, we have developed a technology for calculation and manufacture of phase plates, which allow one to manipulate efficiently the wave front of the terahertz beam. A wave plate, which is designed to obtain the most uniform power distribution with the region 384×6 mm in size, has been calculated, 3D printed, and then studied experimentally. The measurement results agree well with the theoretical predictions. The depth resolution of the image and the dependence of the power profile on the frequency of the electromagnetic radiation have been studied. The beam formed by the plate turned out to be resistant to both deviations in the source frequency in the range 96–97 GHz and variations in the distance between the phase plate and the detection plane in the range 45–65 cm. The possible ways of developing the proposed

technology is to increase the power of the transmitted power by using a different material for 3D printing or modifying the concept of calculations of the plate shape.

This work was supported by the Russian Science Foundation (project No. 19-72-30003).

REFERENCES

1. X.-C. Zhang and J. Xu, *Introduction to THz Wave Photonics*, Springer, New York (2010).
2. S. Wietzke, C. Jansen, C. Jördens, et al., *Proc. SPIE*, **7385**, Art. no. 738506 (2009). https://doi.org/10.1117/12.840991
3. K. Kawase, Y. Ogawa, Y. Watanabe, and H. Inoue, *Opt. Express*, **11**, No. 20, 2549–2554 (2003). https://doi.org/10.1364/OE.11.002549
4. Y. C. Shen, T. Lo, P. F. Taday, et al., *Appl. Phys. Lett.*, **86**, 241116 (2005). https://doi.org/10.1063/1.1946192
5. D. M. Sheen, D. L. McMakin, and T. E. Hall, *IEEE Trans. Microw. Theory Techn.*, **49**, No. 9, 1581–1592 (2001). https://doi.org/10.1109/22.942570
6. V. I. Shashkin, V. L. Vaks, V. M. Danil'tsev, et al., *Radiophys. Quantum Electron.*, **48**, No. 6, 485–490 (2005). https://doi.org/10.1007/s11141-005-0092-8
7. V. F. Vdovin and I. I. Zinchenko, *Radiophys. Quantum Electron.*, **41**, No. 11, 965–979 (1998). https://doi.org/10.1007/BF02676465
8. D. M. Mittleman, *Opt. Express*, **26**. 9417–9431 (2018). https://doi.org/10.1364/OE.26.009417
9. H. Hoshina, Y. Sasaki, A. Hayashi, et al., *Appl. Spectrosc.*, **63**, 81–86 (2009). https://doi.org/10.1366/000370209787169713
10. K. Kawase, R. Yamzaki, K. Imayama, and K. Murate, in: *40th Int. Conf. on Infrared, Millimeter, and Terahertz Waves (IRMMW-THz). August 23–28, 2015, Hong Kong*, p. 1–2. https://doi.org/10.1109/IRMMW-THz.2015.7327583
11. P. Zolliker, M. Shalaby, E. Söllinger, et al., *Sensors*, **21**, No. 11, Art. no. 3757 (2021). https://doi.org/10.3390/s21113757
12. T. J. Smith, A. Broome, D. Stanley, et al., in: *IEEE 45th European Solid State Circuits Conference (ESSCIRC), September 23–26, 2019, Cracow, Poland*, pp. 151–154. https://doi.org/10.1109/ESSCIRC.2019.8902823
13. H. Huang, P. Qiu, S. Panezai, et al., *Opt. Laser Technol.*, **120**, 105683 (2019). https://doi.org/10.1016/j.optlastec.2019.105683
14. D. Čibiraitė, M. Wan, A. Lisauskas, et al., in: *44th Int. Conf. on Infrared, Millimeter, and Terahertz Waves (IRMMW-THz), September 1–6, 2019, Paris, France*, [p. 1–2]. https://doi.org/10.1109/IRMMW-THz.2019.8874217
15. A. V. Shchepetilnikov, P. A. Gusikhin, V. M. Muravev, et al., *Int. J. Infrared Millim. Waves*, **41**, No. 6, 655–664 (2020). https://doi.org/10.1007/s10762-020-00692-4
16. J. He, T. Dong, B. Chi, et al., *J. Infrared Millim. Terahertz Waves*, **41**, 607–631 (2020). https://doi.org/10.1007/s10762-020-00677-3
17. X. Xing, Y. Li, Y. Lu, et al., *Opt. Express*, **27**, A1627–A1635 (2019). https://doi.org/10.1364/OE.27.0A1627
18. J. Gospodarič, A. Kuzmenko, A. Pimenov, et al., *Appl. Phys. Lett.*, **112**, 221104 (2018). https://doi.org/10.1063/1.5027179

19. D. Rohrbach, B. J. Kang, and T. Feurer, *Opt. Express*, **29**, 27160–27170 (2021). https://doi.org/10.1364/OE.433881

20. D. R. Reid and G. S. Smith, *IEEE Trans. Antennas Propag.*, **55**, No. 8, 2138–2146 (2007). https://doi.org/10.1109/TAP.2007.901848

21. S. F. Busch, M. Weidenbach, J. C. Balzer, and M. Koch, *J. Infrared Millim. Terahertz Waves*, **37**, No. 4, 303–307 (2016). https://doi.org/10.1007/s10762-015-0236-7

22. L. Minkevičius, S. Indrišiūnas, R. Šniaukas, et al., *Opt. Lett.*, **42**, 1875–1878 (2017). https://doi.org/10.1364/OL.42.001875

23. R. W. Gerchberg and W. O. Saxton, *Optik*, **35**, No. 2, 237–246 (1972).